Ab initio calculation of phase boundaries in iron along the bcc-fcc transformation path and magnetism of iron overlayers

M. Friák,[1,2] M. Šob,[1,*] and V. Vitek[3]

[1]*Institute of Physics of Materials, Academy of Sciences of the Czech Republic, Žižkova 22, CZ-616 62 Brno, Czech Republic*

[2]*Department of Solid State Physics, Faculty of Science, Masaryk University, Kotlářská 2, CZ-611 37 Brno, Czech Republic*

[3]*Department of Materials Science and Engineering, University of Pennsylvania, 3231 Walnut Street, Philadelphia, Pennsylvania 19104-6272*

A detailed theoretical study of magnetic behavior of iron along the bcc-fcc (Bain's) transformation paths at various atomic volumes, using both the local spin-density approximation (LSDA) and the generalized gradient approximation (GGA), is presented. The total energies are calculated by the spin-polarized full-potential linearized augmented plane waves method and are displayed in contour plots as functions of tetragonal distortion c/a and volume; borderlines between various magnetic phases are shown. Stability of tetragonal magnetic phases of γ-Fe is discussed. The topology of phase boundaries between the ferromagnetic and antiferromagnetic phases is somewhat similar in LSDA and GGA; however, the LSDA fails to reproduce correctly the ferromagnetic bcc ground state and yields the ferromagnetic and antiferromagnetic tetragonal states at a too low volume. The calculated phase boundaries are used to predict the lattice parameters and magnetic states of iron overlayers on various (001) substrates.

Iron exists in both bcc and fcc modifications and has many magnetic phases, especially in thin films. In particular, fcc iron films exhibit a large variety of structural and magnetic properties that depend delicately on the iron layer thickness and preparation conditions.[1–3] The close competition between different magnetic states has also been confirmed by first-principles electronic structure calculations. In the case of Fe, the local spin-density approximation (LSDA) predicts a nonmagnetic close-packed ground state instead of the ferromagnetic bcc phase found in nature.[4,5] It turns out that inclusion of nonlocal effects through the generalized gradient approximation (GGA) overcomes this problem and stabilizes the bcc ferromagnetic state.[5,6] This has also been verified in a number of recent studies (see, e.g., Refs. 7–10).

Recently, Qiu, Marcus, and Ma[11] found that the behavior of the total energy of iron along the tetragonal deformation path at the constant volume of 11.53 Å^3 is quite similar within both LSDA and GGA. As we show in the present paper, the relaxation of volume brings a somewhat different picture of the energetics of iron and, in this way, the similarity mentioned in the above paper is rather a happy coincidence. Very recently, Spišák and Hafner[12] included also the double-layer antiferromagnetic state ($\uparrow\uparrow\downarrow\downarrow$ . . .) into their considerations of energetics of γ-iron multilayers on Cu(001) and found that this magnetic ordering is energetically favored at the lattice constant equal to the equilibrium lattice constant of Cu.

The purpose of this contribution is to perform the calculation of the total energy of iron along the bcc-fcc tetragonal (Bain's) transformation path at various volumes, to identify the stable and metastable phases, and to find the phase boundaries between various iron modifications. This path is significant for energetics of ultrathin films at the (001) substrates, as pseudomorphic epitaxy on a (001) surface of a cubic metal usually results in a strained tetragonal structure of the film. We include ferromagnetic (FM), nonmagnetic (NM), and both single-layer (AFM1 – $\uparrow\downarrow$ . . .) and double-layer (AFMD) antiferromagnetic states. The calculated total energies are used to predict lattice parameters and the type of magnetic ordering of iron layers at various (001) substrates.

Craievich *et al.*[13] have shown that some energy extrema on constant-volume transformation paths are dictated by the symmetry. Namely, most of the structures encountered along the transformation paths between some higher-symmetry structures, say between bcc and fcc at the Bain's path, have a symmetry that is lower than cubic. At those points of the transformation path where the symmetry of the structure is higher the derivative of the total energy with respect to the parameter describing the path must be zero. These are the so-called symmetry-dictated extrema. However, other extrema may occur that are not dictated by symmetry and reflect properties of the specific material. Configurations corresponding to energy minima at the transformation paths represent stable or metastable structures and may mimic atomic arrangements that could be encountered when investigating thin films[14] and extended defects such as interfaces and dislocations.[15,16]

We start with the bcc structure and consider it as a tetragonal one with the c/a ratio equal to 1. Subsequently, we perform a tetragonal deformation (uniaxial deformation along the [001] axis), i.e., we change the c/a ratio and the structure becomes tetragonal. However, at $c/a = \sqrt{2}$, we arrive at the fcc structure, which has again cubic symmetry. The points $c/a = 1$ and $c/a = \sqrt{2}$ correspond to the only high-symmetry structures along the tetragonal deformation path and, therefore, symmetry-dictated extrema of the total energy may be expected here. Let us note here that many papers define the c/a such that the fcc structure is considered a tetragonal one with $(c/a)^* = 1$; then $(c/a)^* = (c/a)/\sqrt{2}$ and the bcc structure corresponds to $(c/a)^* = \sqrt{2}/2$.

We calculate the total energy of NM, FM, AFM1, and AFMD iron along the tetragonal deformation paths keeping
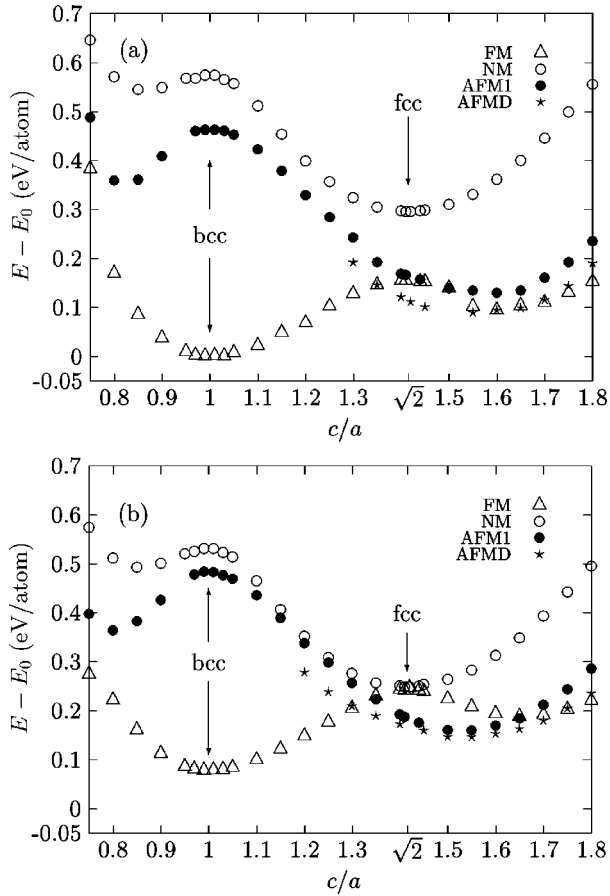
FIG. 1. Variations of total energies of iron along the constant-volume bcc-fcc transformation path for experimental volume $V_{exp} = 11.72$ Å^3 calculated within the GGA (a) and LSDA (b) relative to the equilibrium energy E_0 of FM bcc iron.

FIG. 2. The same as Fig. 1, but for the atomic volume $V = 10.21$ Å^3.

the atomic volume constant; the region of atomic volumes studied extends from $V/V_{exp} = 0.84$ until $V/V_{exp} = 1.05$. For the total-energy calculation, we utilize the full-potential linearized augmented plane waves code described in detail in Ref. 17. The calculations are performed using both the GGA (Ref. 18) and the LSDA.[19] The muffin-tin radius of iron atoms of 1.90 au is kept constant for all calculations, the product of the number of **k**-points and number of nonequivalent atoms in the basis is equal to 6000, and the product of the muffin-tin radius and the maximum reciprocal space vector, $R_{MT}k_{max}$, is equal to 10. The maximum l value for the waves inside the atomic spheres, l_{max}, and the largest reciprocal vector **G** in the charge Fourier expansion, G_{max}, is set to 12 and 15, respectively.

Figures 1(a) and 1(b) display the variation of total energies of iron along the tetragonal deformation path for the experimental lattice volume of the FM bcc iron of 11.72 Å^3 calculated using the GGA and LSDA, respectively. The NM and FM states exhibit energy extrema at $c/a = 1$ and $c/a = \sqrt{2}$ corresponding to higher-symmetry structures (bcc and fcc). However, the AFM1 iron keeps its cubic symmetry only for $c/a = 1$, i.e., for the bcc structure. At $c/a = \sqrt{2}$, the atoms occupy the fcc lattice positions, but as the atoms with spins *up* and *down* are not equivalent, the resulting symmetry
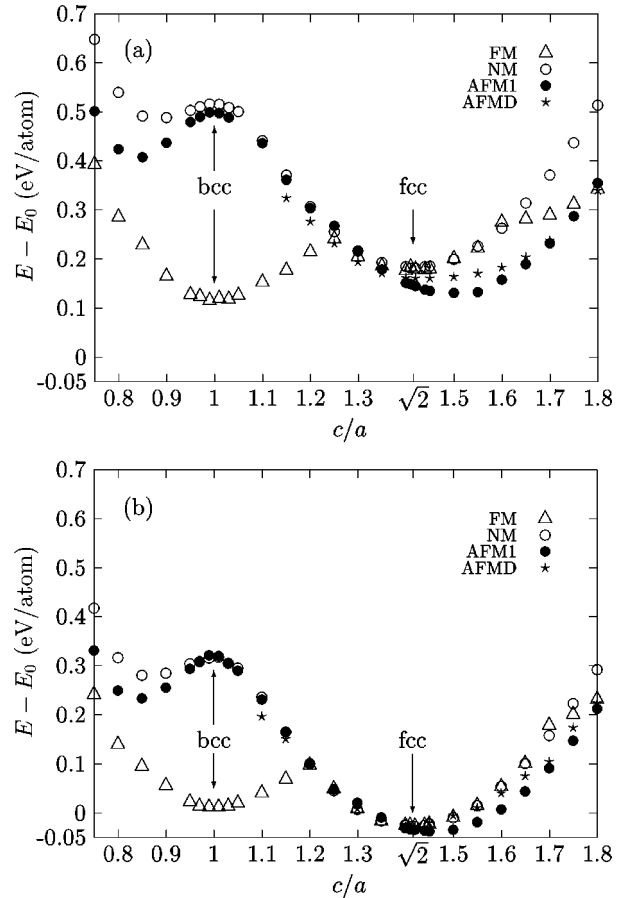
is tetragonal, and no higher-symmetry structure occurs here. Therefore, no symmetry-dictated extremum of total energy at $c/a = \sqrt{2}$ is to be expected. And, indeed, the total-energy curves of AFM1 states exhibit, in general, a nonzero derivative at $c/a = \sqrt{2}$ (Figs. 1 and 2); this was also found by Qiu, Marcus, and Ma.[11] The minima of the AFM1 curves are not dictated by symmetry. As to the AFMD iron, it is never cubic and no symmetry-dictated extrema occur along the tetragonal deformation path.

It may be seen from Figs. 1(a) and 1(b) that the behavior of energies calculated within the GGA and LSDA for the experimental lattice volume is quite alike, in accordance with the findings of Qiu, Marcus, and Ma,[11] who used a slightly different atomic volume of 11.53 Å^3. In both cases, the FM bcc iron has the lowest energy. In the region from $c/a \approx 1.4$ till $c/a \approx 1.7$, the AFMD ordering is most favorable. The shape of the energy curves corresponding to the same type of magnetic order is remarkably similar, but their mutual shift is somewhat different in the GGA and LSDA.

The situation is completely changed at sufficiently lower atomic volumes. Figures 2(a) and 2(b) show the total energies of iron for the atomic volume of 10.21 Å^3. In the GGA, the energy of the FM bcc state is still the lowest one, in contrast to the LSDA case where AFM1 states lie distinctly lower than the FM bcc state. For $1.4 \lesssim c/a \lesssim 1.8$, the AFM1 states are most favorable in both cases. Here the shape of the
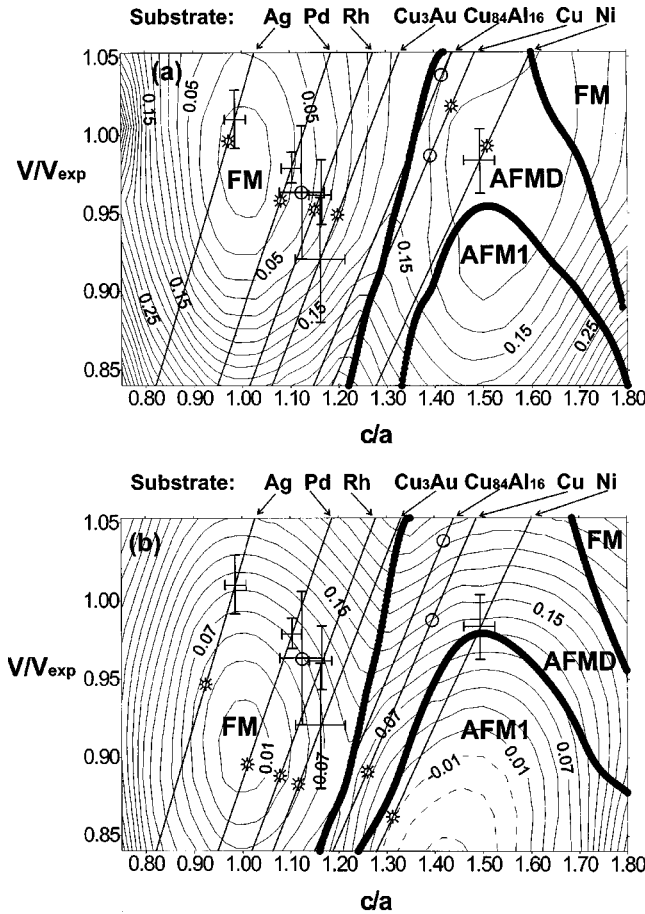
FIG. 3. Total energy of iron as a function of c/a and volume relative to the FM bcc equilibrium state energy calculated within the GGA (a) and LSDA (b). Only states with minimum energy are shown. The contour interval is 20 meV/atom. Thick lines show the FM/AFMD and AFMD/AFM1 phase boundaries. The straight lines correspond to constant lateral lattice parameters of various (001) substrates, as described in the text. The crosses composed from the vertical and horizontal error bars centered at those straight lines represent structures of Fe films on the corresponding substrates found experimentally. One of these crosses is out of the line; it stands for the experimental structure of Fe/Cu₃Au(001) films found in Ref. 27 and its center is denoted by an open circle. The other two open circles show the experimental structures where no error bars were given. Smaller open circles combined with asterisks represent theoretical results found in this work. In Fig. 3(b), the contours with the negative energy (relative to the FM bcc minimum) are drawn by dashed lines.

energy curves corresponding to the same type of magnetic order is quite different in the GGA and LSDA.

The difference between the GGA and LSDA results is seen best in Figs. 3(a) and 3(b), which present contour plots of minimum energies as functions of volume and c/a.[20] We can clearly see the ''horseshoes'' dividing the plane into the AFM1, AFMD, and FM regions. Whereas the GGA reproduces the FM bcc ground state of iron fairly well, the global minimum of energy within the LSDA is, with the volume and c/a as free variables, nonmagnetic fcc, at the volume $V/V_{exp}=0.82$ and about 63 meV/atom below the FM bcc

local minimum [this global minimum is out of the range of Fig. 3(b)].

The AFMD structure may be considered to be a close approximation of the spin-spiral state with $\mathbf{q}=(2\pi/a)(0,0,0.6)$ found as a ground state of the fcc iron.[21] It will be a topic of future studies to show how the noncollinearity of magnetic moments changes in the $(c/a, V/V_{exp})$ plane. We suppose that the region of noncollinear magnetism will not be too much different from the AFMD region shown in Fig. 3(a).

Surprisingly, the positions of borderlines between individual magnetic states are not very different within the GGA and LSDA. This is due to two mutually compensating effects: (i) the whole ''landscape'' of the LSDA is, roughly speaking, shifted to lower volumes with respect to the GGA one (this shifts also the phase boundaries to lower volumes) and, (ii) the local minima and the energy surface in the neighborhood of the fcc structure are shifted to lower energies with respect to the energy surface in the neighborhood of the bcc structure (this shifts the phase boundaries back to higher volumes). The second effect seems to be stronger and, as a result, the phase boundaries in LSDA occur even at higher volumes than in GGA.

Figures 3(a) and 3(b) enable us to predict easily the lattice parameters and magnetic states of iron overlayers at (001) substrates. Let us suppose that the pseudomorphic iron overlayers adopt the lattice dimensions of the substrate in the (001) plane and relax the interlayer distance (characterized by c/a). If the lattice constant of a fcc substrate is equal to a_{sub}, then in the coordinates $x=c/a$, $y=V/V_{exp}$, and $z=E-E_0$, the surfaces corresponding to a fixed a_{sub} in the (001) planes are the planes $y=kx$, where $k=(\sqrt{2}/8)(a_{sub}^3/V_{exp})$. The configuration and magnetic state of iron overlayers on a (001) substrate should correspond to the energy minimum coinstrained to this plane provided that the effect of the substrate/overlayer interface is not very strong.

In Figs. 3(a) and 3(b), these planes for different values of a_{sub} are displayed by straight lines together with available experimental results and our theoretical predictions. Let us discuss the GGA results first [Fig. 3(a)].

The experimental point for Fe films on Ag(001) is taken from Ref. 22. It corresponds to a slightly distorted bcc structure and lies in the FM region, in agreement with experimental findings.[23] Our theoretical point is within the experimental limits. A similar situation takes place for Fe films on Pd(001) (Ref. 24) and Rh(001) (Ref. 25). The films exhibit body centered tetragonal structure and the theoretical results are not very far from the experimental ones (for Rh, we are again within experimental limits). The points for Fe films on Pd and Rh substrates still lie in the FM region. The FM ordering of films on Pd was also confirmed experimentally;[24] as to the Rh substrate, the magnetic structure of the films was not investigated yet.[25]

As for the Cu₃Au(001) substrate, there are two experimental findings for thin films. One of them[26] lies at the straight line for the Cu₃Au substrate in Fig. 3(a), and our theoretical point is within the experimental limits. The other one[27] is somewhat shifted from the Cu₃Au line. The structure

of the films corresponds again to a tetragonally strained FM bcc phase, in agreement with experiment.[27]

Fe films on $Cu_{84}Al_{16}(001)$ are reported to be fcc with the volume of 12.15 $Å^3$.[28] The corresponding point lies very close to the phase boundary between the FM and AFMD ordering in the fcc region. This is also in accordance with experimental findings—up to a 4 ML, high-spin FM state is reported; for higher thicknesses a low-spin and/or AFM phase was found.[28] Here we do not have enough calculated results to find out the theoretical point, but it will not be probably too much higher than $(c/a, V/V_{exp}) = (1.44, 1.05)$.

Another system close to the FM/AFMD phase boundary are the Fe films on Cu(001). This fact confirms a conclusion of Ref. 12 that FM and AFMD phases are energetically almost degenerate along the line corresponding to the lattice constant of Cu and somewhat favored over the AFM1 phase, and is closely connected with a variety of magnetic states found in the Fe films on Cu(001). Our theoretical point lies in the AFMD region and is not very far from the experimental result[29] [see Fig. 3(a)].

Finally, the straight line for Fe films on Ni(001) is, for lower volumes, close to the AFMD/AFM1 phase boundary. However, the experimental point[30] is distinctly in the AFMD region, and our theoretical prediction lies again within the experimental limits. In reality, however, magnetic polarization due to FM Ni substrate may induce FM order in the film.[31]

As may be seen in Fig. 3(b), the LSDA would provide rather wrong theoretical predictions of the lattice parameters of Fe films on metallic substrates. This is due to a considerable shift of the energy minima to the lower volumes.

In conclusion, we have calculated the total energies of iron as a function of volume and tetragonal distortion for various magnetic phases and found the minimum energies both within the GGA and LSDA. The calculated contour plots can be used for the understanding and prediction of lattice parameters and magnetic states of Fe films on various metallic substrates. However, only the GGA gives a favorable agreement with available experimental data.

---

*Corresponding author. Email: mojmir@ipm.cz

[1] H. Jenniches, J. Shen, Ch. V. Mohan, S. S. Manoharan, J. Barthel, P. Ohresser, M. Klaua, and J. Kirschner, Phys. Rev. B **59**, 1196 (1999).

[2] S. J. Lloyd and R. E. Dunin-Borkowski, Phys. Rev. B **59**, 2352 (1999).

[3] D. Schmitz, C. Charton, A. Scholl, C. Carbone, and W. Eberhardt, Phys. Rev. B **59**, 4327 (1999).

[4] C. S. Wang, B. M. Klein, and H. Krakauer, Phys. Rev. Lett. **54**, 1852 (1985).

[5] D. J. Singh, W. E. Pickett, and H. Krakauer, Phys. Rev. B **43**, 11 628 (1991).

[6] P. Bagno, O. Jepsen, and O. Gunnarsson, Phys. Rev. B **40**, 1997 (1989).

[7] L. Stixrude, R. E. Cohen, and D. J. Singh, Phys. Rev. B **50**, 6442 (1994).

[8] E. G. Moroni, G. Kresse, and J. Hafner, Phys. Rev. B **56**, 15 629 (1997).

[9] C. Elsässer, J. Zhu, S. G. Louie, M. Fähnle, and C. T. Chan, J. Phys.: Condens. Matter **10**, 5081 (1998); **10**, 5113 (1998).

[10] H. C. Herper, E. Hoffmann, and P. Entel, Phys. Rev. B **60**, 3839 (1999).

[11] S. L. Qiu, P. M. Marcus, and H. Ma, J. Appl. Phys. **87**, 5932 (2000).

[12] D. Spišák and J. Hafner, Phys. Rev. B **61**, 16 129 (2000).

[13] P. J. Craievich, M. Weinert, J. M. Sanchez, and R. E. Watson, Phys. Rev. Lett. **72**, 3076 (1994).

[14] P. Alippi, P. M. Marcus, and M. Scheffler, Phys. Rev. Lett. **78**, 3892 (1997).

[15] M. Šob, L. G. Wang, and V. Vitek, Comput. Mater. Sci. **8**, 100 (1997).

[16] V. Paidar, L. G. Wang, M. Šob, and V. Vitek, Modell. Simul. Mater. Sci. Eng. **7**, 369 (1999).

[17] P. Blaha, K. Schwarz, and J. Luitz, WIEN97, Technical University of Vienna, 1997 [improved and updated Unix version of the original copyrighted WIEN code, which was published by P. Blaha, K. Schwarz, P. Sorantin, and S. B. Trickey, in Comput. Phys. Commun. **59**, 399 (1990)].

[18] J. P. Perdew, S. Burke, and M. Ernzerhof, Phys. Rev. Lett. **77**, 3865 (1996).

[19] J. P. Perdew and Y. Wang, Phys. Rev. B **45**, 13 244 (1992).

[20] Figures 3(a) and 3(b) are composed of the contour plots for the FM, AFM1, and AFMD states. To ensure sufficient reliability of these plots, they are constructed using the mesh of 25 points along each of the nine tetragonal distortion paths calculated for evenly distributed volumes.

[21] L. M. Sandratskii, Adv. Phys. **47**, 91 (1998).

[22] H. Li, Y. S. Li, J. Quinn, D. Tian, J. Sokolov, F. Jona, and P. M. Marcus, Phys. Rev. B **42**, 9195 (1990).

[23] M. Stampanoni, A. Vaterlaus, M. Aesschliman, and F. Meier, Phys. Rev. Lett. **59**, 2483 (1987).

[24] J. Quinn, Y. S. Li, H. Li, D. Tian, F. Jona, and P. M. Marcus, Phys. Rev. B **43**, 3959 (1991).

[25] A. M. Begley, S. K. Kim, F. Jona, and P. M. Marcus, Phys. Rev. B **48**, 1786 (1993).

[26] B. Feldmann, B. Schirmer, A. Sokoll, and M. Wutig, Phys. Rev. B **57**, 1014 (1998).

[27] B. Schirmer, B. Feldmann, and M. Wutig, Phys. Rev. B **58**, 4984 (1998).

[28] W. A. Macedo, F. Sirotti, G. Panaccione, A. Schatz, W. Keune, W. N. Rodrigues, and G. Rossi, Phys. Rev. B **58**, 11 534 (1998).

[29] S. H. Lu, J. Quinn, D. Tian, F. Jona, and P. M. Marcus, Surf. Sci. **209**, 364 (1989).

[30] G. C. Gazzadi, P. Luches, A. di Bona, L. Marassi, L. Pasquali, S. Valeri, and S. Nannarone, Phys. Rev. B **61**, 2246 (2000).

[31] B. Schirmer and M. Wutig, Phys. Rev. B **60**, 12 945 (1999).